Supporting Information

Decahedral Platinum−Copper Nanoframes Enriched with Defects for Highly Efficient Electrocatalytic Hydrogen Evolution Reaction

Xueying Cao, Fuhe Le*, Pengfei Hu, Xue Yang, Dianzeng Jia, Wenming Sun*, Wei Jia*

X. Cao, X. Yang, D. Jia, and W. Jia

State Key Laboratory of Chemistry and Utilization of Carbon Based Energy Resources; College of Chemistry, Xinjiang University, Urumqi, 830017, Xinjiang, China

F. Le

Xinjiang Key Laboratory of New Energy Materials and Green Chemical Engineering, Engineering Department of Chemistry and Environment, Xinjiang Institute of Engineering, Urumqi, Xinjiang 830091, P. R. China

P. Hu

School of Materials Science and Engineering, Shanghai University, Shanghai, 200444, PR China

W. Sun

Department of Chemistry, Beijing Key Laboratory for Optical Materials and Photonic Devices, Capital Normal University, Beijing 100048, China

* Corresponding authors. E-mail addresses: jxxjlfh@126.com (F. Le); swm@mail.sdu.edu.cn (W. Sun); jia3816892@163.com (W. Jia)

1. Experimental details

Materials.

Platinum (II) acetylacetonate ($Pt(acac)_2$, 97%), Copper (II) chloride dihydrate ($CuCl_2 \cdot 2H_2O$) and glucose were purchased from Aladdin. Oleylamine ($CH_3(CH_2)_7CH=CH(CH_2)_7CH_2NH_2$, OAm) was purchased from Acros Organics and oleic acid ($CH_3(CH_2)_7CH=CH(CH_2)_7COOH$, OA) was obtained from Sinopharm Chemical Reagent Co., Ltd (Shanghai, China). Nafion solution (5 wt.%) was obtained from Sigma-Aldrich. Commercial Pt/C (20 wt.%) was purchased from Alfa Aesar. All the chemicals in this work were directly used without further purification.

Synthesis of Pt–Cu NFs and PtCu-X.

In a typical synthesis, the Pt–Cu NFs were generated by simultaneously injecting 10 mg $Pt(acac)_2$, 50 mg $CuCl_2 \cdot 2H_2O$ and 60 mg glucose into a mixture of OA and OAm. A blue-green solution was obtained, which was subjected to 30 min of ultrasonic treatment and then stirred in the 180 ℃ oil bath for 240 min. After cooling to room temperature, the product was collected by centrifugation and successively washed with cyclohexane and ethanol several times, followed by vacuum drying for 6 h. To investigate the effect of reaction time, samples were synthesized at different reaction times (40, 70, 100, and 120 min) and are denoted as PtCu-X, where X represents the reaction time in minutes.

Treatment of Pt–Cu NFs/C catalysts.

Conductive carbon black (20 mg) was dispersed in ethanol (20 mL) and Pt–Cu NFs/-X catalysts (2 mg) mentioned above were added simultaneously. After stirring at ambient conditions for 36 h, the black suspension was centrifuged. In order to remove the residual OAm and OA from the surface of the material, the centrifuged catalysts were dispersed in 30 mL of acetic acid solution and refluxed at 80 ℃ for 12 h. The final catalysts were washed three times with ethanol and then vacuum-dried at 60 ℃ for 8 h.

Preparation of the Pt–Cu NFs electrode.

The mixture of 2.5 mg of Pt–Cu NFs/C catalysts, 20 μL of Nafion solution (5 wt.%) and 480 μL of ethanol was ultrasonicated for 1 h to obtain a uniformly dispersed ink solution. Then 10 μL of the catalyst inks were dropped onto glassy carbon electrode

(GCE) and dried in the air. To further remove the residual OAm and OA, the GCE was exposed to 254 nm of UV light for 10 h. The catalysts loading was determined to be 0.25 mg cm^{-2}.

Preparation of the Pt/C electrode.

2.5 mg commercial Pt/C (20 wt.%), 20 μL Nafion solution and 480 μL ethanol were mixed and ultrasonicated for 1 h to obtain a uniformly dispersed ink solution. Subsequently, the suspension was dropped onto GCE and then dried in the air.

Materials Characterizations.

X-ray diffraction (XRD) results were carried out using a D8 Bruker diffractormeter with Cu Kα as radiation source. The morphology and three-dimensional structure of as-prepared materials were observed using high-Resolution transmission electron microscopy (HRTEM) (JEM-2100F). The high-angle annular dark-field scanning electron microscope (HAADF-STEM) (Titan) was employed to collect microstructures and elemental mappings at atomic resolution of samples. Scanning electron microscope energy-dispersive X-ray spectroscopy (SEM-EDS) was performed on Hitachi SU8010 at an accelerating voltage of 20 kV. X-ray photoelectron spectroscopy (XPS) with Al Kα excitation source (ESCALAB 250Xi) was conducted to obtain the valence information of the samples. The content of Cu in electrolytes was detected using inductively coupled plasma mass spectrometry (ICP-MS, Agilent 7800). The content of Pt loading was detected by inductively coupled plasma-optical emission spectrometry (ICP-OES, PerkinElmer Optima 8000). X-ray absorption fine structure (XAFS) spectroscopy was carried out using the Rapid XAFS 2M (Anhui Absorption Spectroscopy Analysis Instrument Co., Ltd.). Using Si (771) and Si (553) spherically bent crystal analyzer with a radius of curvature of 500 mm for Pt and Cu by transmission mode at 20 kV and 20 mA. The acquired XAFS spectra were processed and analyzed using the Demeter software package (version 0.9.26). [1]

Electrochemical measurements.

All of HER measurements were performed on a CHI 760E electrochemical workstation (CH Instruments, Shanghai) employing a conventional three-electrode configuration (Ag/AgCl electrode as the reference electrode, graphite rod as the counter

electrode and GCE modified with Pt–Cu NFs, PtCu-X catalysts and Pt/C as working electrode) in 0.5 M H_2SO_4 electrolyte. The GCE should be polished with Al_2O_3 paste carefully and ultrasonic cleaning in deionized water for 5~10 s before each experiment. Electrochemical cyclic voltammetry detection was conducted between -0.1 V and -0.7 V (vs. Ag/AgCl electrode) with a scan rate of 100 mV s^{-1} to activate electrode. The activity of the electrodes was evaluated by linear sweep voltammetry (LSV) curves with 100% IR compensation. The potentials should be referenced to a reversible hydrogen electrode (RHE) as following: $E_{RHE} = E_{Ag/AgCl} + 0.059pH + 0.1989$. Electrochemical impedance spectroscopy (EIS) was measured from 0.1 Hz to 100 kHz. The HER durability of Pt–Cu NFs was carried out through comparing the LSV curve before and after 2000 CV. The chronoamperometry measurements was examined under a constant 100 mA cm^{-2} for 500 h to evaluate the stability.

The ECSA was calculated via the desorption region of underpotential deposition hydrogen (H_{upd}) in CV curve[2]:

$$ECSA = \frac{Q_H}{0.21\ (mC \cdot cm^{-2}) \cdot m_{Pt}}$$

where Q_H represents electron transfer quantity (the hydrogen desorption peak), m_{Pt} is the mass loading of noble metals on the working electrode, $0.21\ mC \cdot cm^{-2}$ is the theoretical value of a one-electron transfer assuming on H atom per Pt surface atom. Specifically, the Pt loadings in Pt–Cu NFs were measured to be 15.65 wt.%.

The number of active sites (n) can be obtained:

$$n = \frac{Q_H}{2F}$$

where F is the Faraday constant (96485 C mol^{-1}).

The turnover frequency (TOF) was calculated using the formula below:

$$TOF = \frac{I}{2nF}$$

where I represents for the current (A) during the linear sweep measurement, F is the Faraday constant (96485 C mol^{-1}), and n is the number of active sites (mol).

MEA measurements.

Prior to the fabrication of MEAs, the Nafion 115 membrane was treated with 5% H_2O_2, 0.5 M H_2SO_4, and deionized water at 80 ℃ for 2 h, respectively. The treated membrane was then preserved in deionized water for further use. Pt–Cu NFs (350 μg_{Pt} cm^{-2}) and commercial Pt/C (500 μg_{Pt} cm^{-2}) were applied as cathode catalysts and IrO_2 was used as anode catalyst. The anodic catalyst is commercial IrO_2 with a loading of 2.0 mg cm^{-2}. The catalyst ink was prepared by sonicating the mixture of catalysts (Pt–Cu NFs, Pt/C, and IrO_2), 5 wt.% Nafion ionomer, deionized water and isopropanol. A self-made cell was used as the PEMWE device and Ti mesh was applied as anodic gas diffusion layers (GDLs), carbon paper as cathodic GDLs. Then a certain quality of ink was sprayed onto GDLs. All PEMWEs were operated at 65 ℃ and the reactant was deionized water circulated via the peristaltic pump (15 ml min^{-1}). All the data of PEMWE were not iR corrected.

Density functional theory (DFT) calculations.

Quantum-Espresso package[3] was used to simulate the structural and electronic properties of the interface. The generalized gradient approximation (GGA) with spin-polarized Perdewn-Burke-Ernzerhof (PBE) scheme[4] was employed for calculating the exchange and correlation function. The core electrons were represented by the PAW data-set from pslibrary (https://dalcorso.github.io/pslibrary/)[5]. After convergence testing, kinetic energy cutoff and charge density cutoff were set at 40 Ry and 200 Ry, respectively. The Fermi-surface effects were treated by the smearing technique of degauss, using a smearing parameter of 0.05 Ry. The model was constructed based on 4-layers 4*4 Cu (111) slab. Within the top two layers of the slab, several Cu atoms were replaced with Pt atoms to simulate the isolated Pt sites according to the structural information derived from EXAFS measurements. During the structure optimization, the atoms of bottom two layers were frozen, while the atoms of top two layers and the adsorbate were allowed to relax until the forces vanished within 0.027 eV/Å.

The free energy of H atom adsorbed on different sites is defined as:

$\Delta G_{H^*} = \Delta E_H - \Delta E_{ZPE} + T\Delta S$

where ΔE_H is the adsorption energy of H atom based on DFT calculation, ΔE_{ZPE} and

ΔS are the differences of zero-point energy and entropy between adsorption structure and gas phase H_2. ΔE_H is defined as:

$\Delta E_H = E_{tot} - E_{sub} - 1/2E_{H2}$

Where E_{tot} is the total energy of hydrogen adsorbed system, E_{sub} and E_{H2} is the energy of substrate and H_2 molecule.

2. Supporting figures and tables

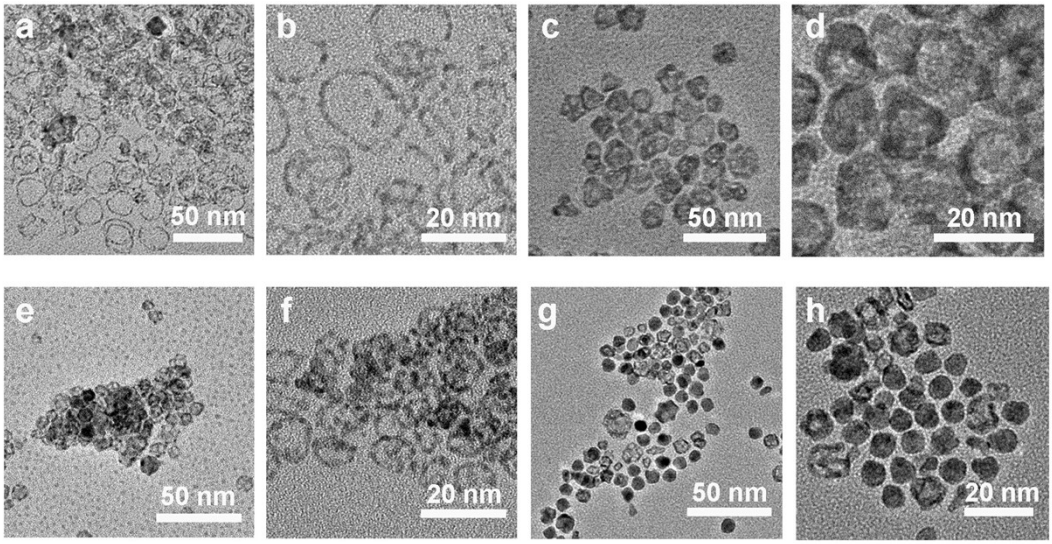

Figure S1. TEM images of products synthesized under the identical conditions for preparation of Pt–Cu NFs except different volume ratio of OAm/OA. (a, b) 9 mL/1 mL. (c, d) 8 mL/2 mL. (e,f) 7 mL/3 mL. (g, h) 5 mL/5 mL.

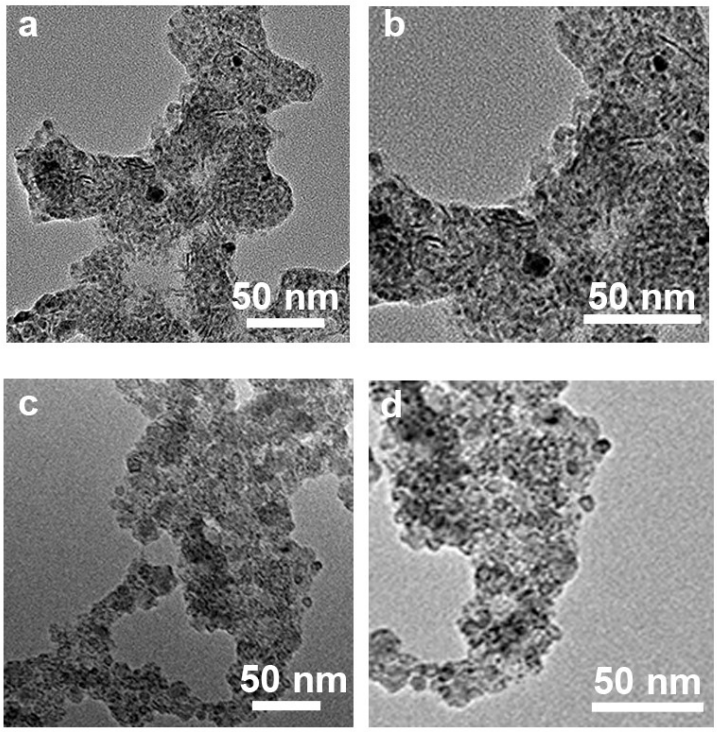

Figure S2. TEM images of products synthesized under the identical conditions for preparation of Pt–Cu NFs except different reaction temperature. (a, b) 110 ℃ (c, d) 160 ℃.

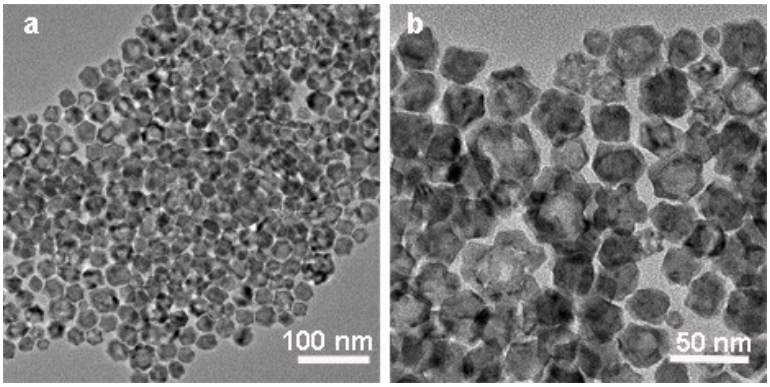

Figure S3. (a-b) TEM images of products synthesized under the identical conditions for preparation of Pt–Cu NFs with potassium hexachloroplatinate (K_2PtCl_6) as Pt source.

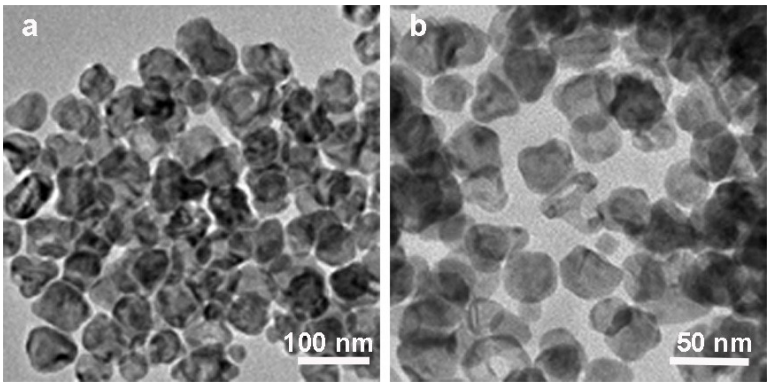

Figure S4. (a-b) TEM images of products synthesized under the identical conditions for preparation of Pt–Cu NFs except with 8 mg of $Pt(acac)_2$.

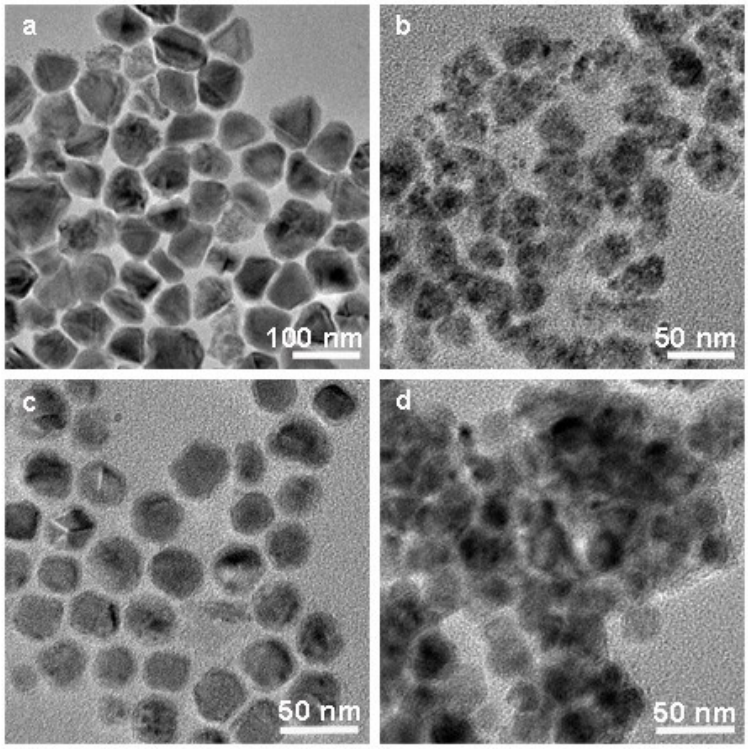

Figure S5. TEM images of products synthesized under the identical conditions for preparation of Pt–Cu NFs except different Cu sources. (a) $Cu(NO_3)_2 \cdot 6H_2O$. (b) $Cu(acac)_2$. (c) $CuSO_4 \cdot 5H_2O$. (d) $Cu(CH_3COO)_2 \cdot H_2O$.

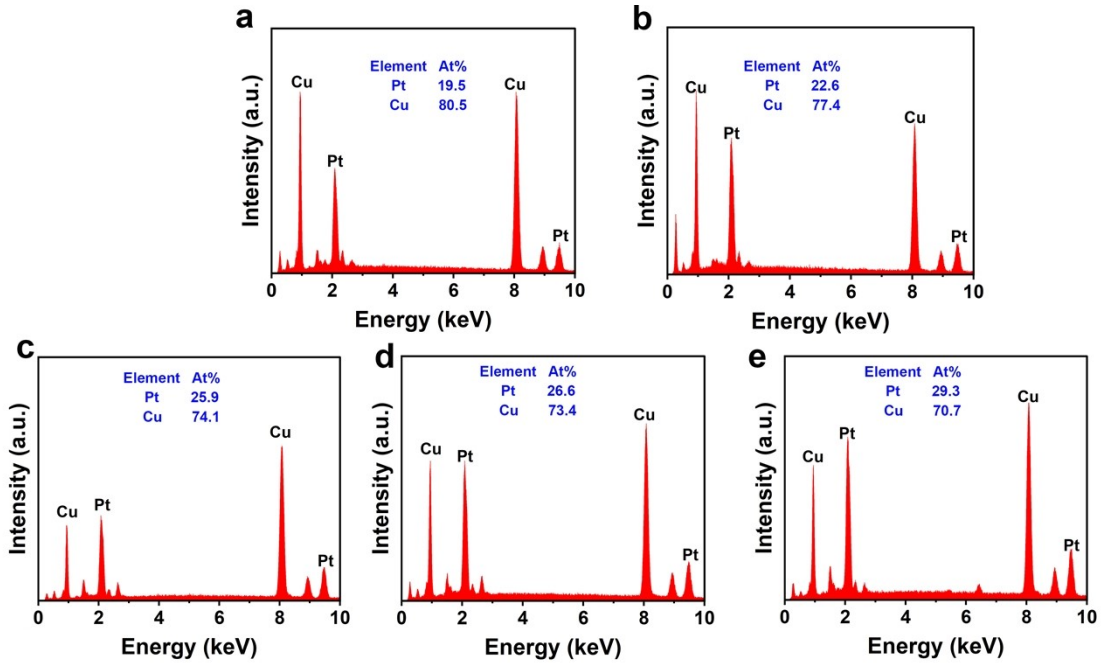

Figure S6. SEM-EDS images of intermediates obtained after the reaction proceeding for (a) 40 min, (b) 70 min, (c) 100 min, (d) 120 min, (e) 240 min.

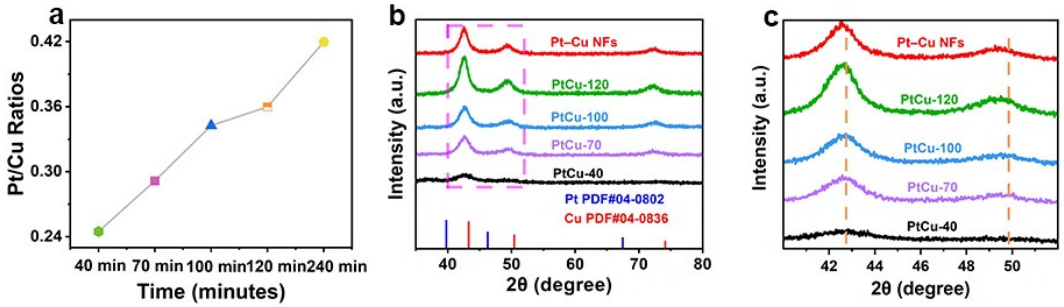

Figure S7. (a) Atomic ratio changes of Pt and Cu in different intermediates, as determined by SEM-EDS. (b) XRD patterns and (c) enlarged XRD patterns of these intermediates.

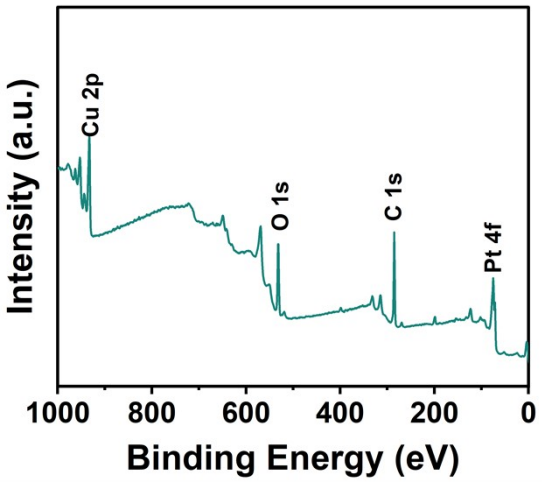

Figure S8. XPS survey spectrum of Pt–Cu NFs.

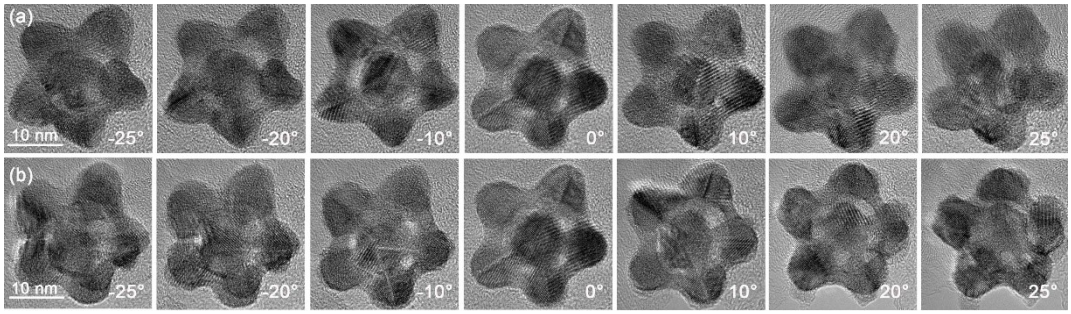

Figure S9. The HRTEM images of Pt–Cu NFs rotating along the X (up) and Y (down) axes.

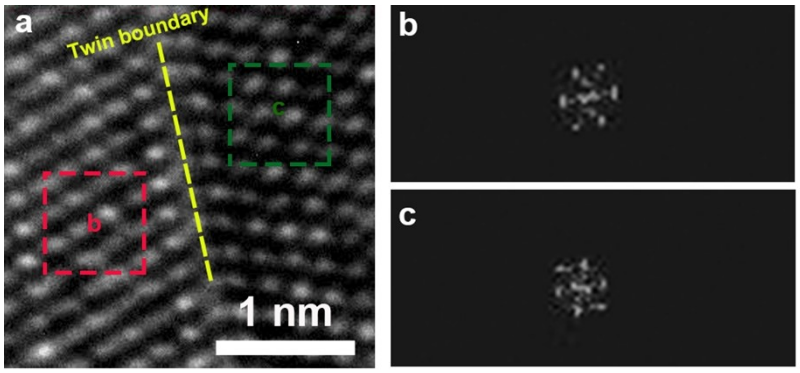

Figure S10. (a) HRTEM image of a Pt–Cu NFs taken out from a sample prepared, (b, c) FFT patterns of the Pt–Cu NFs corresponding to different regions shown in (a).

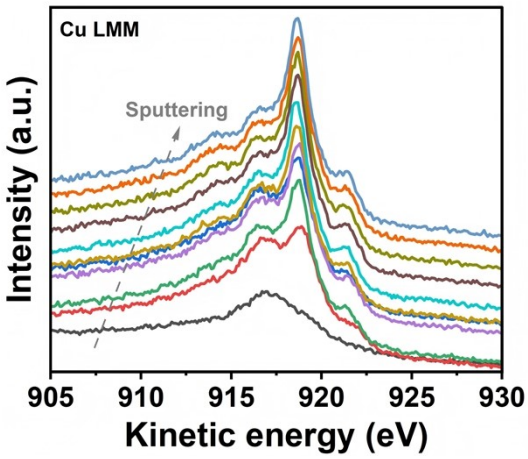

Figure S11. Cu LMM XPS in-depth analyses of Pt–Cu NFs with different sputtering time.

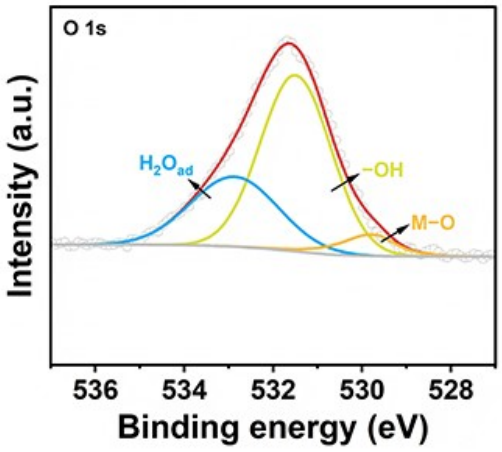

Figure S12. High-resolution O 1s spectrum of Pt–Cu NFs.

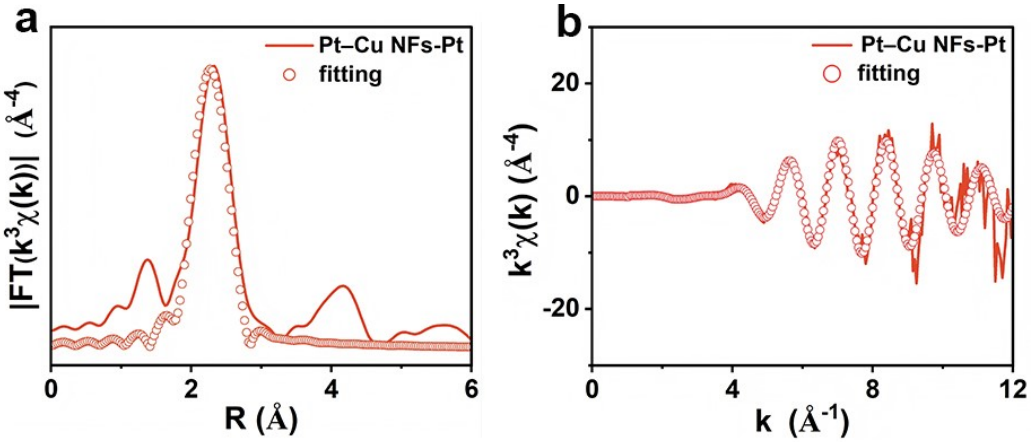

Figure S13. (a) EXAFS fitting curve of Pt–Cu NFs (Pt) at R-space. (b) FT-EXAFS fitting curve of Pt–Cu NFs (Pt) at k-space.

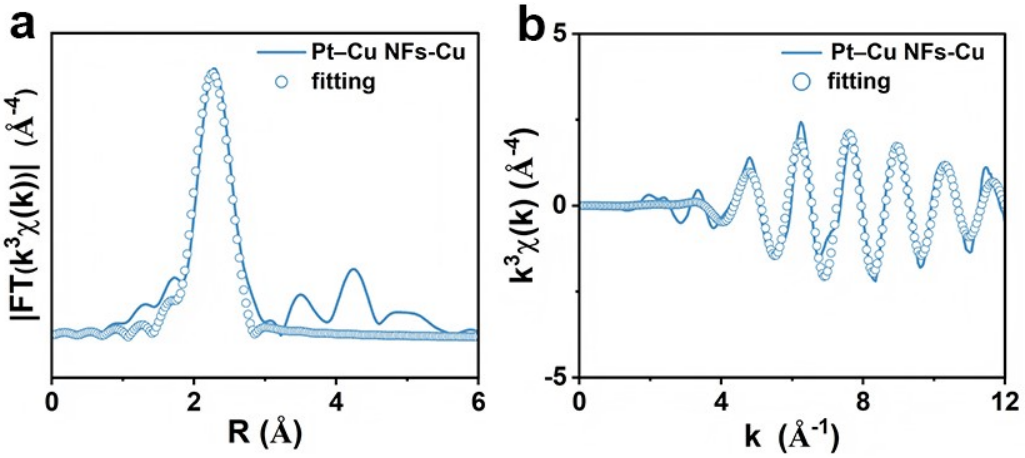

Figure S14. (a) EXAFS fitting curve of Pt–Cu NFs (Cu) at R-space. (b) FT-EXAFS fitting curve of Pt–Cu NFs (Cu) at k-space.

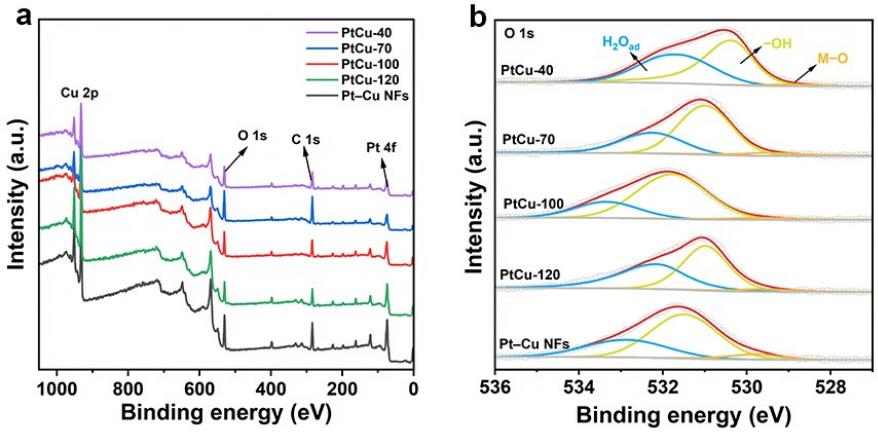

Figure S15. (a) Survey XPS spectra. (b) High-resolution XPS spectra of O 1s for PtCu alloy catalysts.

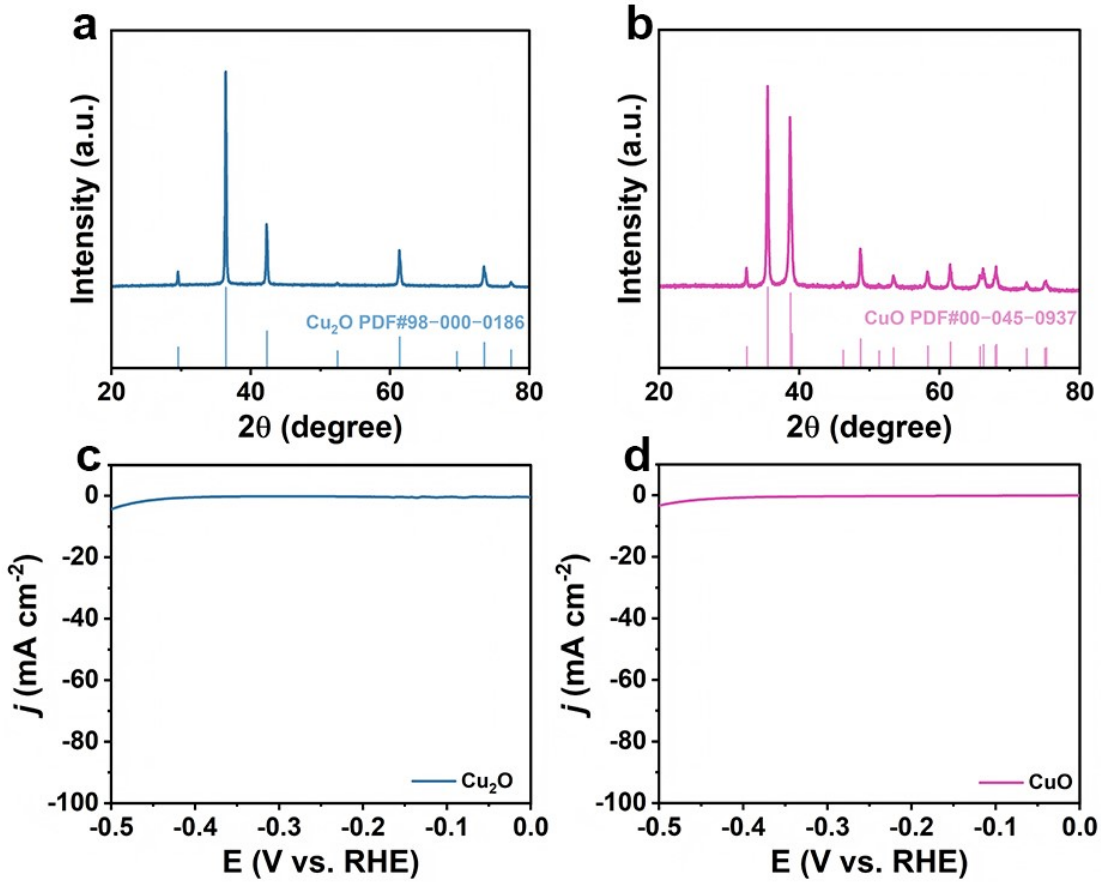

Figure S16. XRD patterns of (a) Cu_2O and (b) CuO. LSV curves of (c) Cu_2O and (d) CuO.

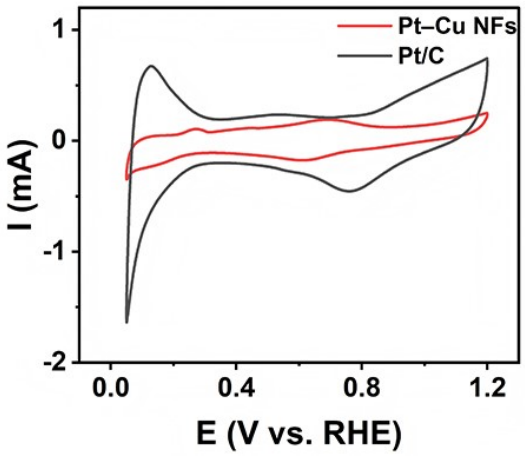

Figure S17. CV curves of Pt–Cu NFs and Pt/C.

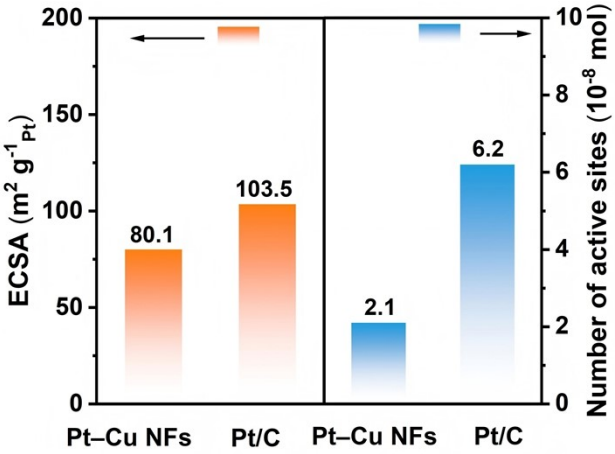

Figure S18. Comparison of ECSA values and number of active sites for Pt–Cu NFs and Pt/C.

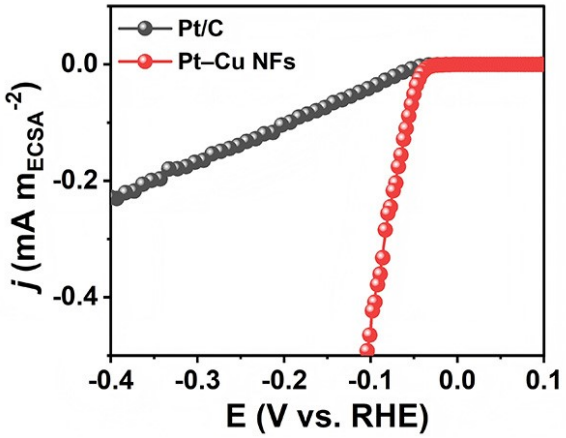

Figure S19. ECSA-normalized HER polarization curves of Pt–Cu NFs and Pt/C.

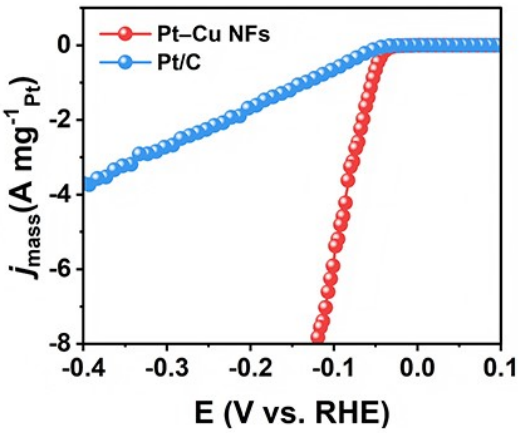

Figure S20. LSV curves normalized to loading of Pt.

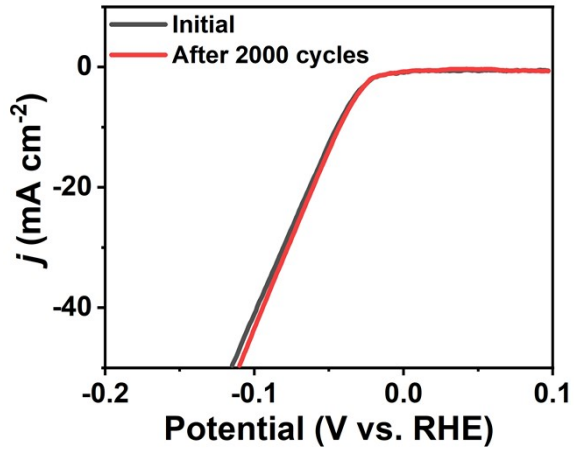

Figure S21. The polarization curves of the Pt–Cu NFs before and after 2,000 continuous cycles.

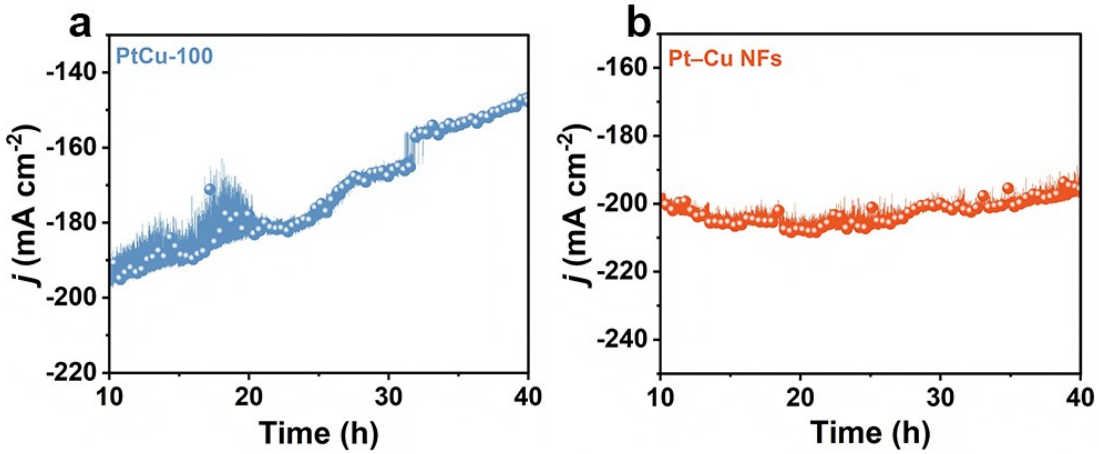

Figure S22. The i-t curves of (a) PtCu-100 and (b) Pt–Cu NFs.

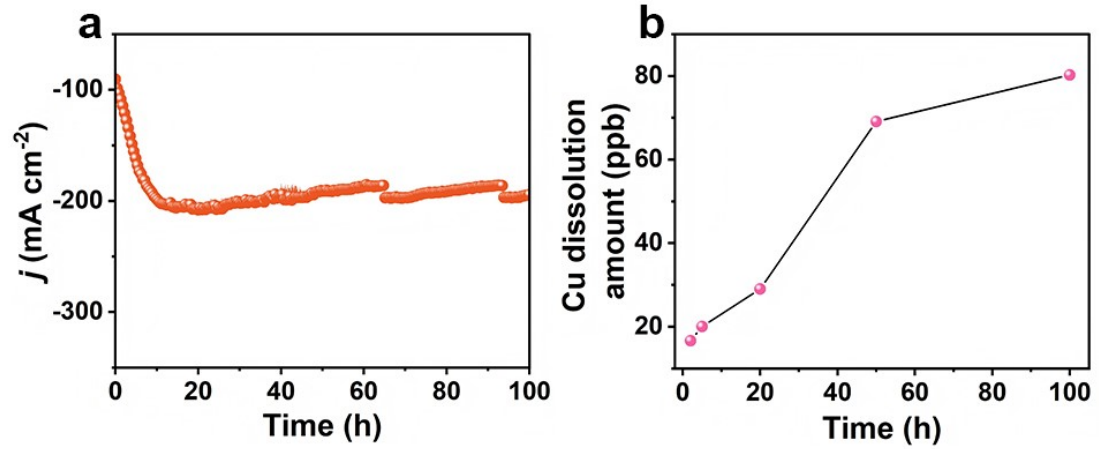

Figure S23. (a) The i-t curve of Pt–Cu NFs. (b) Dissolution of Cu during the stability tests.

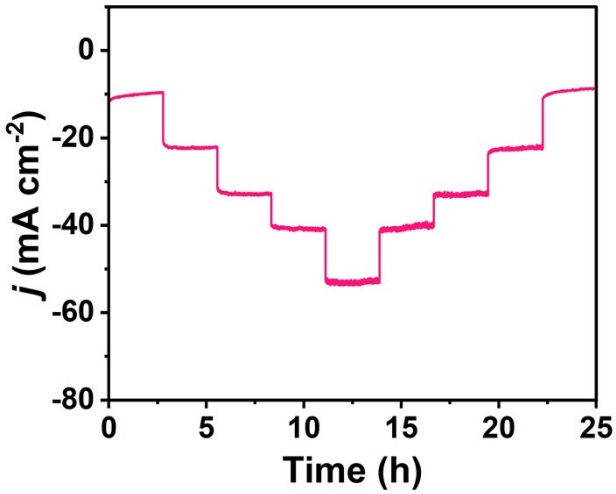

Figure S24. Multi-current chronoamperometry of Pt–Cu NFs from 10 to 50 mA cm^{-2} at current ramps of 10 mA cm^{-2} pre step.

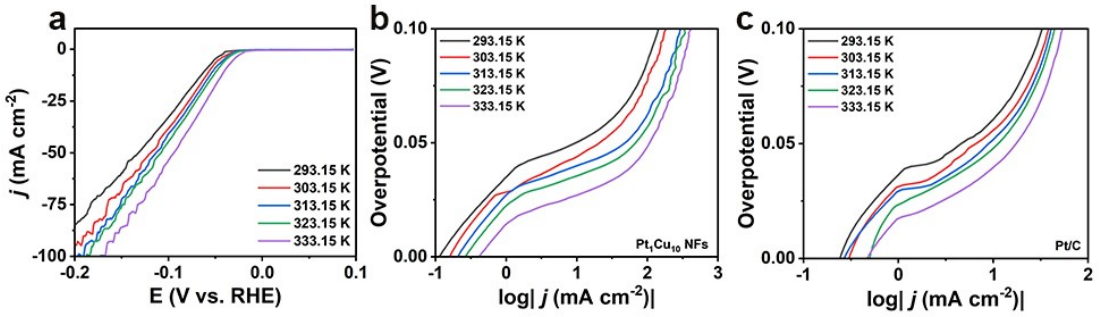

Figure S25. (a) Polarization curves of Pt/C under the temperature range of 293.15-333.15 K. (b) Tafel plots of Pt–Cu NFs under the temperature range of 293.15-333.15 K. (c) Tafel plots of Pt/C under the temperature range of 293.15-333.15 K.

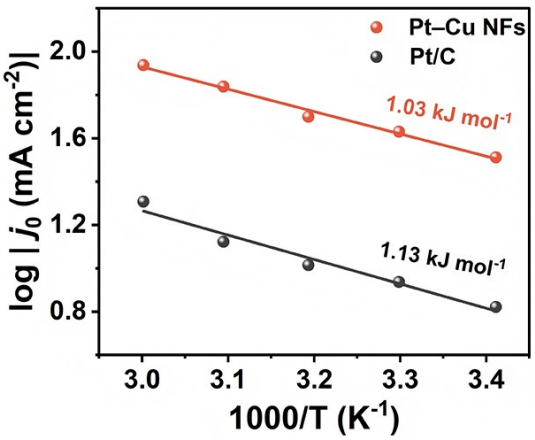

Figure S26. Arrhenius plots of Pt–Cu NFs and Pt/C.

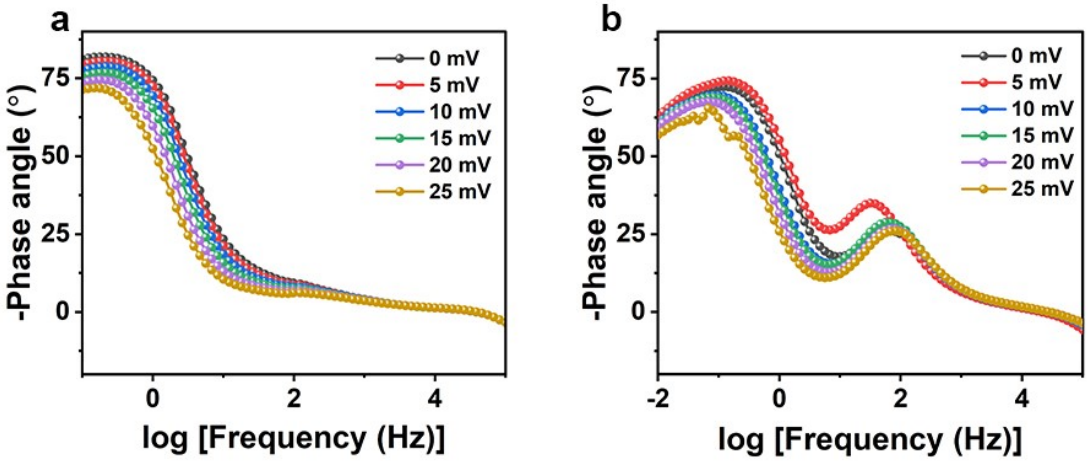

Figure S27. Bode phase plots of the in-situ EIS for (a) Pt–Cu NFs and (b) Pt/C.

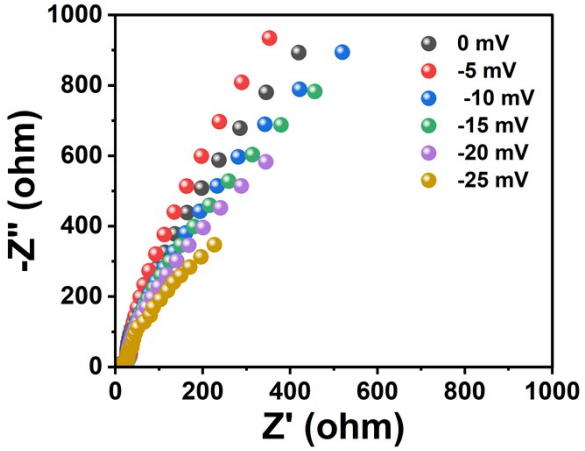

Figure S28. Nyquist curves of Pt/C at various potentials.

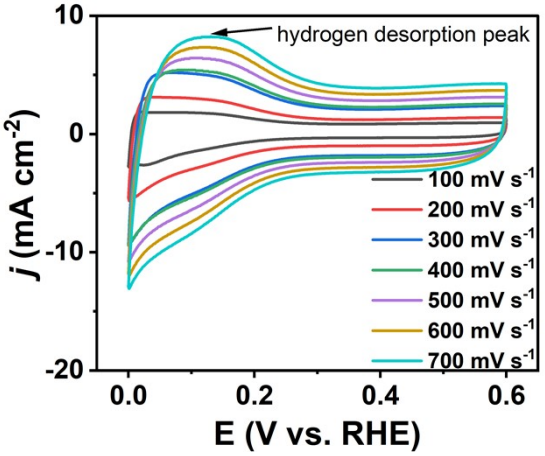

Figure S29. CV profiles of Pt/C with the scan rate from 100 to 700 mV s^{-1}.

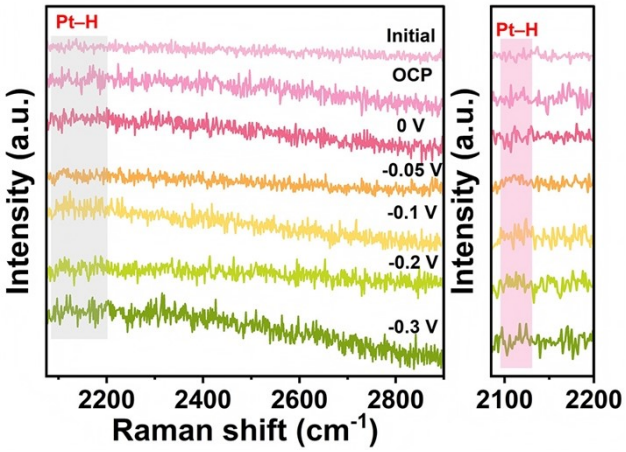

Figure S30. In-situ Raman spectra of Pt–Cu NFs recorded in 0.5 M H_2SO_4 from OCP to −0.3 V (vs. RHE).

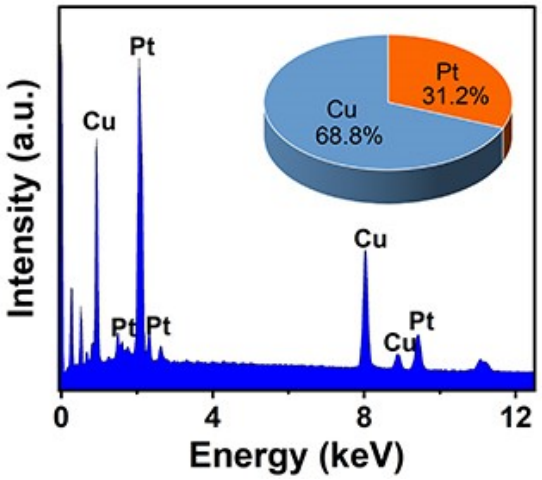

Figure S31. SEM-EDS of Pt–Cu NFs after the HER.

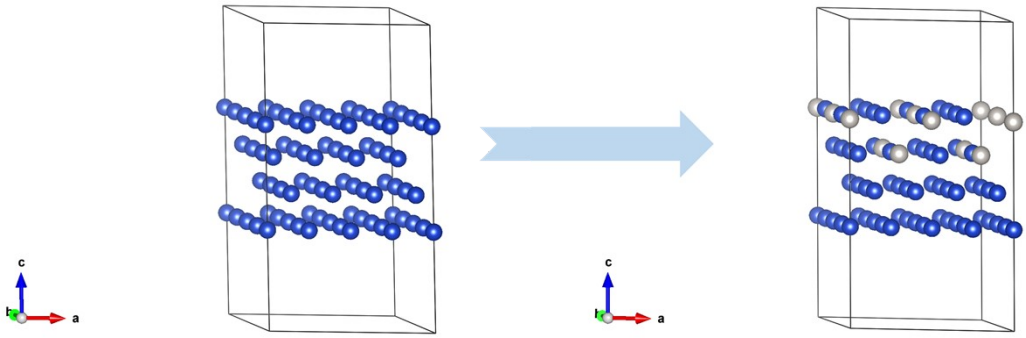

Figure S32. The side-view of the model structure before and after Pt doping.

Table S1. EDS and XPS results of the Pt and Cu contents for the as-prepared catalysts.

Catalysts	Overall Pt/Cu atomic ratio (EDS)	Surface Pt/Cu atomic ratio (XPS)
PtCu-40	19.50/80.50	19.40/80.60
PtCu-70	22.60/77.40	21.13/78.87
PtCu-100	25.90/74.10	23.72/76.28
PtCu-120	26.60/73.40	25.05/74.95
Pt–Cu NFs	29.30/70.70	29.82/70.18

Table S2. EXAFS fitting parameters of Pt–Cu NFs at Pt L_3-edge and Cu for various samples. (S_0^2=1)

Sample	**Shell**	**CN**	**R (Å)**	**σ^2(Å^2)**	**ΔE_0 (eV)**	***R* factor**
Pt foil	Pt-Pt	12.0*	2.76	0.0037	6.7	0.0067
Cu foil	Cu-Cu	12.0*	2.54	0.0087	3.9	0.0012
Pt–Cu NFs	Pt-Cu	8.3	2.61	0.0084	4.4	0.0244
	Cu-Cu	1.8	2.55	0.0087	9.9	0.0248

CN is the coordination number; R is interatomic distance (the bond length between central atoms and surrounding coordination atoms); σ^2 is Debye-Waller factor (a measure of thermal and static disorder in absorber-scatterer distances); ΔE_0 is edge-energy shift (the difference between the zero kinetic energy value of the sample and that of the theoretical model); R factor is used to value the goodness of the fitting.

Table S3. Summary of charge-transfer resistances (R_{ct}) of the PtCu-40, -70, -100, -120, Pt–Cu NFs and commercial Pt/C.

Catalysts	**R_{ct} (Ω)**
PtCu-40	164.8
PtCu-70	44.7
PtCu-100	32.3
PtCu-120	34.1
Pt–Cu NFs	7.2
Pt/C	15.7

Table S4. Comparisons of catalytic performance of the Pt–Cu NFs catalyst in this work and the representative Pt-based catalysts reported in the literatures.

Electrocatalysts	Overpotential (mV)	Tafel slope (mV dec^{-1})	References
Pt–Cu NFs	10.4	33.3	This work
Pt SA/m-WO_{3-x}	47	45	[6]
Pt1@Fe-N-C	60	42	[7]
S-M-5Pt	62	78	[8]
EG-Pt/CoP	21	42.5	[9]
Pt_1/NMHCS	40	56	[10]
Pd@Ru(111) THs	48	51	[11]
PtS_2/Ti_2C	55	60	[12]
Ag@Pt	49	64.1	[13]
PtCu/WO_3@CF	41	45.9	[14]
F-SnO_2@Pt	42	34	[15]
Pt@Ni_2-rGO	37	43	[16]
Pt_1/OLC	38	36	[17]

Table S5. EIS simulation fitting results of Pt–Cu NFs.

η (mV)	R_s (Ω)	CPE-T	CPE-P	R_1 (Ω)	R_2(Ω)	$C_φ$ (F)
0	6.26	0.0005	1.07	4.43	3841	0.0064
-5	6.23	0.0004	1.09	3.56	1481	0.0067
-10	6.19	0.0005	1.06	3.36	1022	0.0078
-15	6.16	0.0009	0.99	3.62	719	0.0099
-20	6.20	0.0022	0.92	4.64	494	0.0157
-25	6.20	0.0079	0.72	4.75	333	0.034

Table S6. EIS simulation fitting results of Pt/C.

η (mV)	R_s (Ω)	CPE-T	CPE-P	R_1 (Ω)	R_2(Ω)	$C_φ$ (F)
0	6.52	0.0004	0.96	18.99	17793	0.0028
-5	6.45	0.0004	0.96	12.31	14687	0.0036
-10	6.39	0.0005	0.91	11.55	5296	0.0050
-15	6.34	0.0007	0.87	10.10	4273	0.0069
-20	6.22	0.0011	0.79	8.97	1004	0.0107
-25	5.98	0.0037	0.62	9.13	421	0.0211

3. References

[1] B. Ravel, and M. Newville, *J. Synchrotron Radiat.*, 2005, **12**, 537-541.

[2] J. Li, J. Liu, C. Chen, J. Guo, R. Bi, S. Chen, L. Zhang, and M. Zhu, *Chem. Eng. J.*, 2022, **436**, 135186.

[3] P. Giannozzi, S. Baroni, N. Bonini, M. Calandra, R. Car, C. Cavazzoni, D. Ceresoli, G. L. Chiarotti, M. Cococcioni, I. Dabo, A. Dal Corso, S. de Gironcoli, S. Fabris, G. Fratesi, R. Gebauer, U. Gerstmann, C. Gougoussis, A. Kokalj, M. Lazzeri, L. Martin-Samos, N. Marzari, F. Mauri, R. Mazzarello, S. Paolini, A. Pasquarello, L. Paulatto, C. Sbraccia, S. Scandolo, G. Sclauzero, A. P. Seitsonen, A. Smogunov, P. Umari, and R. M. Wentzcovitch, *J. Phys.: Condens. Matter*, 2009, **21**, 395502.

[4] Perdew, Burke, and Ernzerhof, *Phys. Rev. Lett.*, 1996, **77**, 3865-3868.

[5] A. Dal Corso, *Comput. Mater. Sci.*, 2014, **95**, 337-350.

[6] J. Park, S. Lee, H.-E. Kim, A. Cho, S. Kim, Y. Ye, J. W. Han, H. Lee, J. H. Jang, and J. Lee, *Angew. Chem., Int. Ed.*, 2019, **58**, 16038-16042.

[7] X. Zeng, J. Shui, X. Liu, Q. Liu, Y. Li, J. Shang, L. Zheng, and R. Yu, *Adv. Energy Mater.*, 2018, **8**, 1701345.

[8] C. Cui, R. Cheng, H. Zhang, C. Zhang, Y. Ma, C. Shi, B. Fan, H. Wang, and X. Wang, *Adv. Funct. Mater.*, 2020, **30**, 2000693.

[9] J. Li, H.-X. Liu, W. Gou, M. Zhang, Z. Xia, S. Zhang, C.-R. Chang, Y. Ma, and Y. Qu, *Energy Environ. Sci.*, 2019, **12**, 2298-2304.

[10] P. Kuang, Y. Wang, B. Zhu, F. Xia, C.-W. Tung, J. Wu, H. M. Chen, and J. Yu, *Adv. Mater.*, 2021, **33**, 2008599.

[11] K. Su, H. Zhang, S. Qian, J. Li, J. Zhu, Y. Tang, and X. Qiu, *ACS Nano*, 2021, **15**, 5178-5188.

[12] S. Jeong, H. D. Mai, T. K. Nguyen, J.-S. Youn, K.-H. Nam, C.-M. Park, and K.-J. Jeon, *Appl. Catal., B*, 2021, **293**, 120227.

[13] L. Yang, R. Grzeschik, P. Jiang, L. Yu, C. Hu, A. Du, S. Schlücker, and W. Xie, *Angew. Chem., Int. Ed.*, 2023, **62**, e202301065.

[14] L. Liu, Y. Wang, Y. Zhao, Y. Wang, Z. Zhang, T. Wu, W. Qin, S. Liu, B. Jia, H. Wu, D. Zhang, X. Qu, M. Chhowalla, and M. Qin, *Adv. Funct. Mater.*, 2022, **32**,

2112207.

[15] T. Kim, S. B. Roy, S. Moon, S. Yoo, H. Choi, V. G. Parale, Y. Kim, J. Lee, S. C. Jun, K. Kang, S.-H. Chun, K. Kanamori, and H.-H. Park, *ACS Nano*, 2022, **16**, 1625-1638.

[16] W. Xu, J. Chang, Y. Cheng, H. Liu, J. Li, Y. Ai, Z. Hu, X. Zhang, Y. Wang, Q. Liang, Y. Yang, and H. Sun, *Nano Res.*, 2022, **15**, 965-971.

[17] D. Liu, X. Li, S. Chen, H. Yan, C. Wang, C. Wu, Y. A. Haleem, S. Duan, J. Lu, B. Ge, P. M. Ajayan, Y. Luo, J. Jiang, and L. Song, *Nat. Energy*, 2019, **4**, 512-518.